Nuclear Instruments and Methods in Physics Research A250 (1986) 244–253
North-Holland, Amsterdam

EXPERIMENTAL RESULTS OF NONRELATIVISTIC ELECTRON BEAM TRAPPING AND ENERGY TRANSFER IN A COMPTON SCATTERING FREE ELECTRON LASER SCHEME

R.Z. OLSHAN, A. GOVER, S. RUSCHIN, H. KLEINMAN, A. FRIEDMAN, B. STEINBERG and I. KATZ

Faculty of Engineering, Tel-Aviv University, Ramat-Aviv, 69978 Israel

We report the first observation of electron trapping and the energy transfer effect induced by two counter-propagating laser beams. The beam sources were two CO_2 transversely excited lasers, operating at 9.3 μm and 10.6 μm, respectively, generating a ponderomotive potential with a short period (about 5 μm). The electron beam had an energy of 1–1.3 keV, corresponding to a velocity in resonance with the ponderomotive potential created by the laser beams. A decelerating axial electric field of 62 V/m was applied in the interaction region. Trapped or quasi-trapped electrons were not fully decelerated by the axial field, allowing energy differentiation between these and the untrapped electrons. Trapping efficiencies of up to 25% were measured, and the laser-induced increase in energy (nondeceleration) ranged between 0 and 5 eV. The measured laser to electron energy transfer resonance curve may be explained by either multimode quasi-trapping or by the phase displacement energy transfer and energy spread processes.

1. Introduction

In the reported experiment, electrons from a nonrelativistic (1 keV) beam were successfully trapped or quasi-trapped by a 5 μm wavelength ponderomotive potential produced by two counter-propagating intense CO_2 laser beams, operating at different wavelengths. During the 150 ns pulse of the lasers, the electrons trapped by the ponderomotive pontential did not experience the deceleration of an applied axial electric field. It was thus possible to detect the trapped electrons by means of a retarding potential, which only permitted the trapped electrons (those with increased energy) to arrive at the collector. Initial measurements indicate a trapping efficiency of up to 25%, with a 50 μA electron beam current which had an energy spread of approximately 6 eV.

In free electron lasers (FELs), amplification of the electromagnetic wave occurs as a result of stimulated Compton scattering from an electron propagating in a transverse periodic magnetic field wiggler [1–3]. Saturation of this radiative emission process occurs when electrons are trapped in the throughs of the ponderomotive potential wave [4,5]. Once fully trapped by the field, the electrons propagating with a constant phase velocity cease to emit radiation.

In order to improve the efficiency of FELs, additional energy can be extracted after saturation by the application of an axial accelerating electric field [6,7], or by tapering of the magnetic wiggler [8,9]. The present experiment will provide useful information on nonlinear (saturation) characteristics of FEL interactions, electron trapping effects and electron trapping efficiencies, and hence will provide information on the physical processes in electromagnetically pumped FELs and in efficiency enhanced schemes of FELs, such as wiggler tapering or axial electric field application.

The experimental setup will be used in particular, to study the effects of wave incoherence and electron insertion parameters on the trapping efficiency. Other possible applications are: accurate measurements of electron energy distribution, axial electron velocity selection and analysis, and fast optical modulation of electron currents.

2. Experimental concept

The experimental concept is illustrated in fig. 1, and described in more detail in ref. [11]. A nonrelativistic electron beam is accelerated to a selected energy (1.0–1.3 keV), and directed along the optical axis of two counter-propagating CO_2 laser beams. The electrons are linearly decelerated (or accelerated) by means of an external axial electric field, which results from the Ohmic potential drop due to a current pulse applied to a coil surrounding the electron beam. The coil current also produces an axial magnetic field that serves to focus and to guide the electron beam along the optical axis.

The signal laser operates at 9.3 μm and propagates along the optical axis in the direction of the electron beam. The wiggler field is produced by a laser operating at 10.6 μm, and propagates in the opposite direction to the signal field and to the electron beam. The combined

0168-9002/86/$03.50

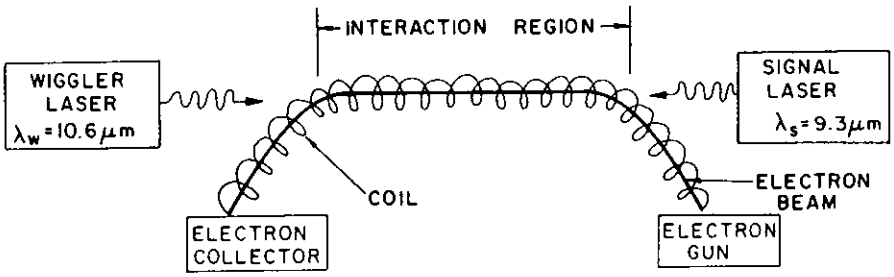

Fig. 1. Schematics of electron trapping experiment concept.

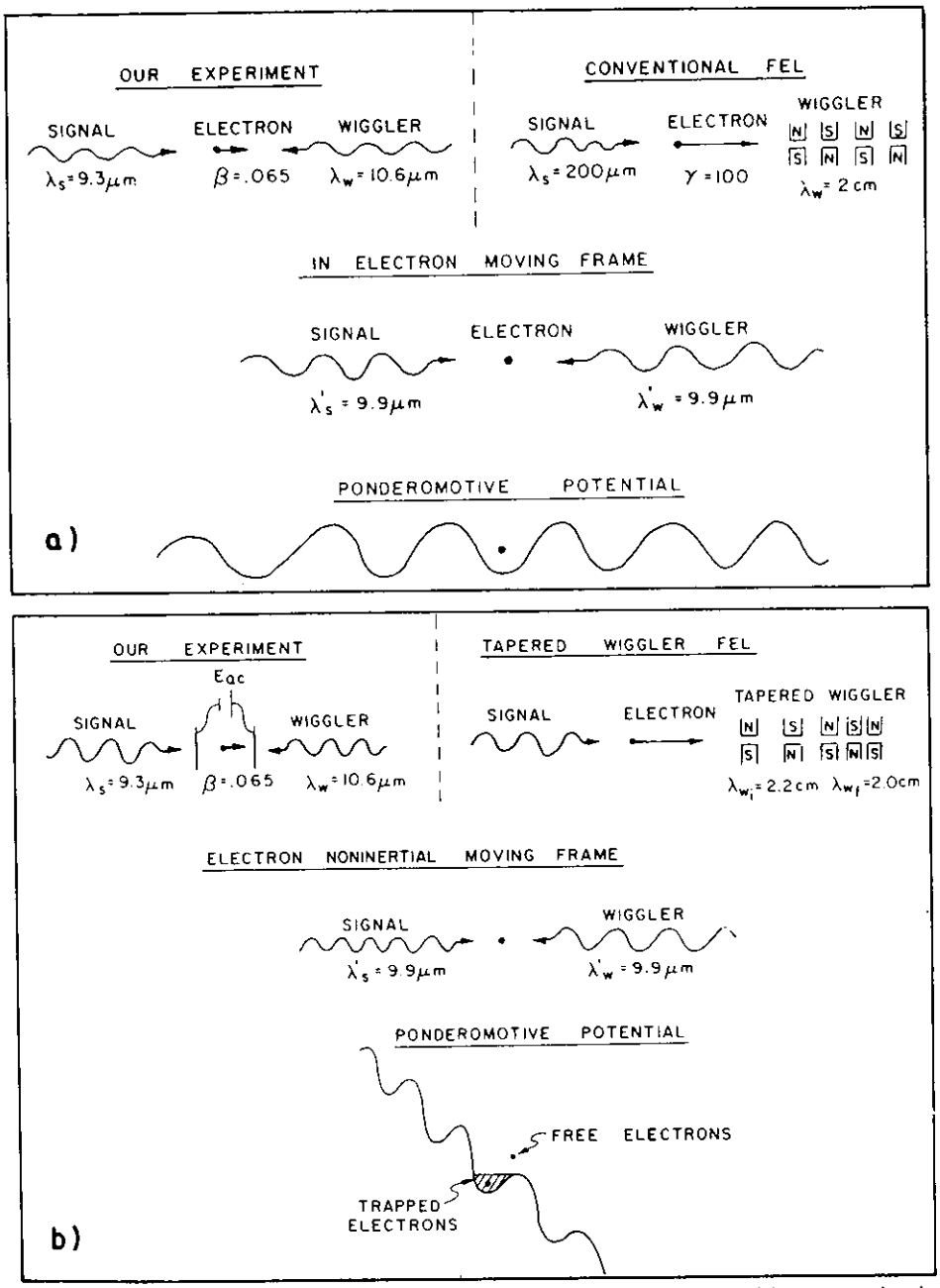

Fig. 2. Analogy between the electron interaction situation in our experiment and in a magnetic wiggler FEL: (a) No axial electric field present vs periodic wiggler; (b) Application of axial electric field vs wiggler tapering.

action of the transverse electromagnetic field of the laser beams produces a ponderomotive wave:

$$E_p(z, t) = |E_p| \sin[(\omega_s - \omega_w)t - (k_s + k_w)z], \quad (1)$$

where $|E_p|$ is the magnitude of the ponderomotive potential, ω_s and ω_w are the frequencies of the signal and wiggler lasers, and k_s and k_w are the wave numbers of the signal and wiggler lasers, respectively. This ponderomotive wave propagates at the phase velocity β_{ph}:

$$\beta_{ph} = \left(\frac{1}{c}\right)\frac{\omega_s - \omega_w}{k_s + k_w} = \frac{\lambda_w - \lambda_s}{\lambda_w + \lambda_s}. \quad (2)$$

The velocity of the electrons is adjusted to be in resonance with the ponderomotive wave at the entrance to the interaction region (the region where the electron beam and two laser beams overlap).

In the moving frame of reference of the ponderomotive wave, the two electromagnetic waves appear to approach the electron with the same Doppler shifted wavelength:

$$\lambda'_w = \lambda'_s = \lambda_w\sqrt{\frac{1-\beta_{ph}}{1+\beta_{ph}}} = 9.90\ \mu\text{m}. \quad (3)$$

In the moving frame, the ponderomotive potential wave appears to be a static axial field:

$$E'_p(z') = |E'_p| \sin(k'z'), \quad (4)$$

where

$$\lambda' = \frac{2\pi}{k'} = \frac{\lambda'_w}{2} = \frac{\lambda'_s}{2} = 4.95\ \mu\text{m}. \quad (5)$$

In a conventional static wiggler FEL with $\lambda_s = 200$ μm, $\lambda_w = 2$ cm, and $\gamma = 100$, the Doppler shifted signal and wiggler wavelengths will appear in the ponderomotive wave frame the same as those encountered in our experiment, as illustrated in fig. 2a.

The axial electric field will decelerate free electrons while in the interaction region. If, however, the electrons become trapped in the troughs of the ponderomotive wave, they will propagate along with the wave, and thereby receive additional energy from the electromagnetic waves. Alternatively, if the axial electric field were to accelerate the electrons, the trapped electrons would release energy by radiating, thus providing optical gain to the signal field. This is analogous to a tapered wiggler FEL, as illustrated in fig. 2b.

Energy analysis is performed on the electron beam upon exiting the interaction region by means of a retarding potential. With a slightly negative potential at the collector, only the trapped electrons have sufficient energy to be detected. The electron energy distribution is obtained by scanning the retarding potential.

3. Theory

The concept of electron trapping is most transparent in the moving frame of the ponderomotive potential wave. An analysis of this kind has been previously reported [9–11]. Here we present a summary of an alternative derivation, in the laboratory frame, of the electron equations of motion in the presence of the two counter-propagating signal and wiggler electromagnetic waves and an external axial electric field.

The signal and wiggler electromagnetic fields are given by:

$$E_w = \text{Re}\left[|\tilde{E}_w|\hat{e}_w\, e^{-i\omega_w t - ik_w z}\right], \quad (6)$$

$$E_s = \text{Re}\left[|\tilde{E}_s|\hat{e}_s\, e^{-i\omega_s t + ik_s z}\right], \quad (7)$$

where $\tilde{E}_w$, $\tilde{E}_s$ are the transverse fields, $\hat{e}_w$, $\hat{e}_s$ are the polarization unit vectors, ω_w, ω_s are the wiggler and signal wave frequencies, and k_w, k_s are the wiggler and signal wave numbers.

The axial force equation for an electron is derived from the Lorentz force equation

$$\frac{d}{dt}(\gamma m_e v_z) = -eE_p(z, t) - eE_{ac}, \quad (8)$$

where $E_p(z, t)$ is the ponderomotive field given by:

$$E_p(z, t) = \text{Re}\left[|\tilde{E}_p|\hat{e}_z\ \exp(-i\psi)\right], \quad (9a)$$

where

$$|\tilde{E}_p| = e\eta_0\frac{\hat{e}_w\hat{e}_s^*}{\pi c^2\gamma_r m_e}(\lambda_s + \lambda_w)\frac{\sqrt{P_s P_w}}{w_{0s}w_{0w}}, \quad (9b)$$

where η_0 is the free space impedance, P_s, P_w are the signal and wiggler peak laser powers, w_{0s}, w_{0w} are the signal and wiggler laser beam widths, $\psi = \omega t - kz$ is the electron phase, $\omega = \omega_s - \omega_w$ and $k = k_s + k_w$, and γ_r is the electron energy at resonance with the ponderomotive wave.

Integrating the force equation (8), we obtain

$$(\delta\gamma)^2 = (\delta\gamma_{max})^2 + \tfrac{1}{2}(\delta\gamma_t^0)^2[\cos\psi + (\psi - \psi_r)\sin\psi_r - \cos\psi_r], \quad (10)$$

where $\delta\gamma_{max} = \delta\gamma_t^0\sqrt{\cos\psi_r + (\psi_r - \text{II}_2)\sin\psi_r}$ is the maximum energy of the trap, ψ_r is the electron phase at resonance with the ponderomotive wave given by:

$$\psi_r = \arcsin\left(\frac{E_{ac}}{E_p}\right). \quad (11)$$

E_{ac} is the applied axial electric field and

$$\delta\gamma_t^0 = \sqrt{\frac{e\beta_r^2\gamma_r^3|E_p|}{\beta_0 mc^2}}$$

is the half-width of the trap with no external field applied, where $\beta_r = \sqrt{1 - \gamma_r^2}$.

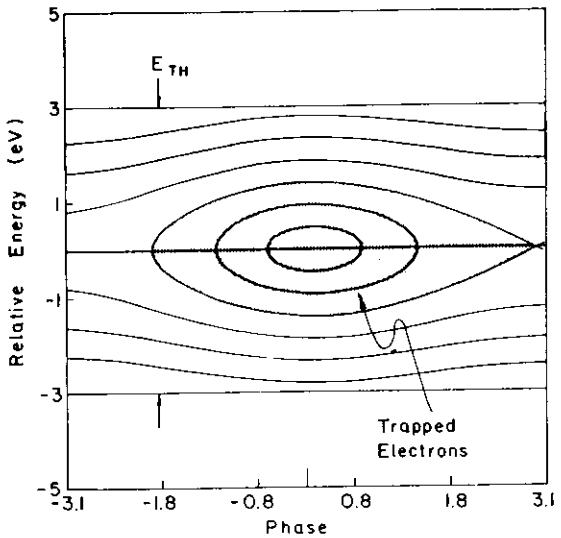

Fig. 3. Electron orbits in phase space.

Solutions of the equation of motion, as illustrated in fig. 3, show various electron energy–phase paths under the influence of the ponderomotive potential in the presence of the axial electric field.

The trapped electrons are those that have closed orbits. The largest of the closed orbits is defined as the separatrix.

The trapping efficiency (η) is calculated by the ratio of the integral of the separatrix ($F_{sep}(\psi_r, \psi)$) to the area defined by the thermal energy spread $\Delta\gamma$, and the initial phase distribution (assumed to be uniform):

$$\eta = \frac{A_{sep}}{2\pi\Delta\gamma}. \tag{12}$$

The area of the separatrix is

$$A_{sep} = 2\,|\delta\gamma_t^0| \int_{\psi_1}^{\pi-\psi_r} F_{sep}(\psi_r, \psi)\,\mathrm{d}\psi, \tag{13}$$

where

$$F_{sep}(\psi_r, \psi) = \sqrt{0.5\big(\cos\psi_r + (\psi + \psi_r - \pi)\sin\psi_r + \cos\psi\big)}\,. \tag{14}$$

4. Experiment description and operation

A schematic of the experiment is illustrated in fig. 4. Details of the electron optical system were previously reported [11]. One main modification in the electron optical system, as compared with the previously reported one, was the removal of the time of flight tube. Energy analysis is now performed by means of a retarding potential. The following is a description of the experiment operation.

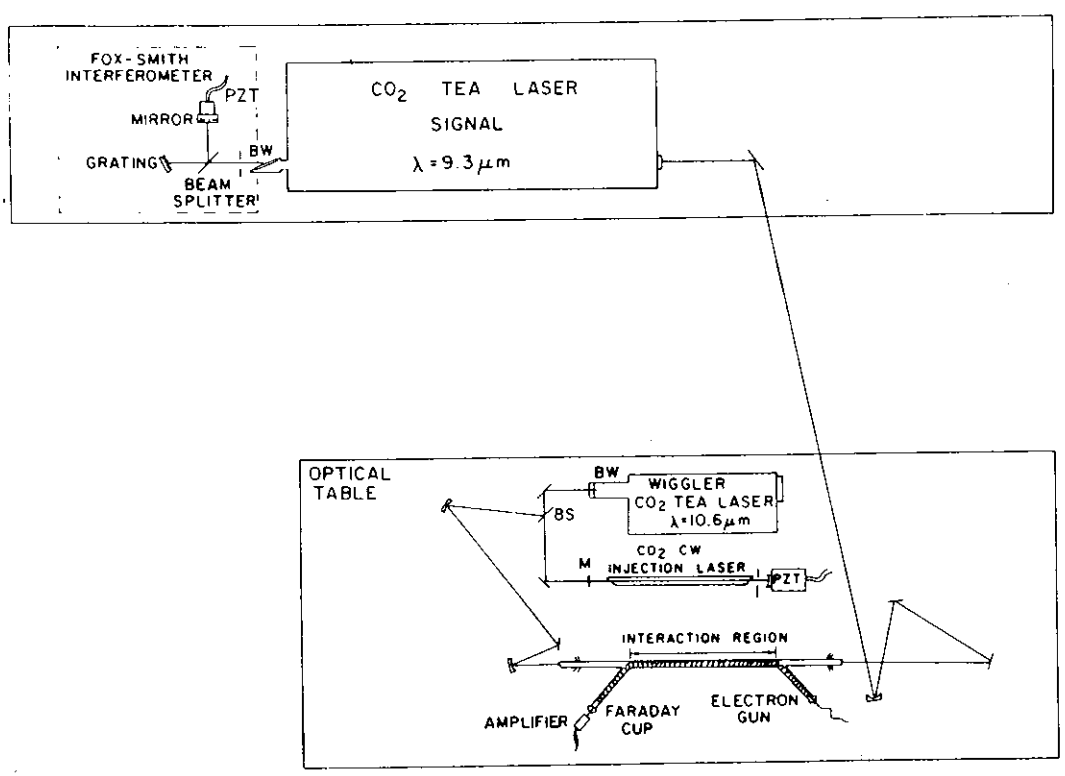

Fig. 4. Experiment schematic.

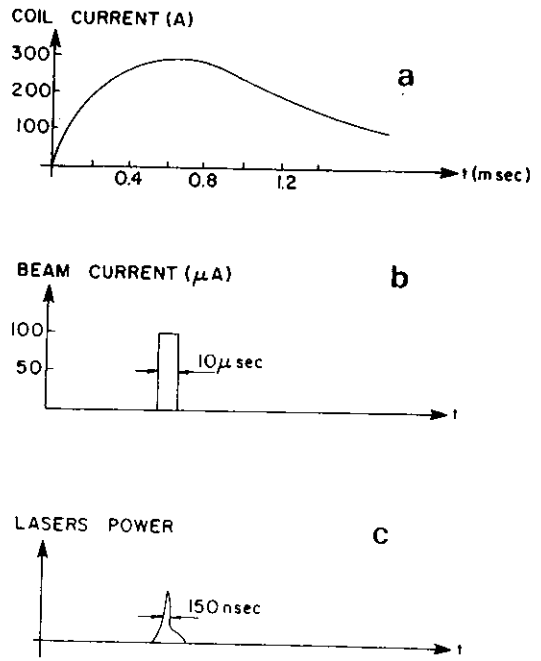

Fig. 5. Timing diagrams of pulses involved in the experiment: (a) Coil current; (b) Electron pulse; (c) Laser pulse.

The experiment is initiated when a current pulse of 500 μs duration is applied to the coil (fig. 5). This copper wire coil serves several functions in the experiment. First, the coil current generates an axial magnetic field (1–2 kG), which guides the electron beam along the optical axis. Secondly, the finite Ohmic resistance of the copper wire generates a potential drop, resulting in an axial electric field (62 V/m), which linearly accelerates or decelerates the electrons (depending on the coil current direction) throughout the interaction region. In addition, the coil aids in EMI shielding of the electron beam and defines the potential surrounding the electrons.

The electron source is a Pierce gun designed for a traveling wave tube. At the peak of the coil current pulse, the electron gun emits a 50–100 μA current pulse of 10 μs duration. The electrons are initially accelerated to an energy between 1.0 and 1.3 keV in order to achieve resonance at a particular location along the interaction region. Upon exiting the interaction region, the electrons are decelerated to allow retarding potential energy analysis, whereby the collector current is measured while scanning the retarding potential. Prior to each experimental trial, a positive potential (approximately 20 V) is applied to the retarding electrode to measure the total current. The retarding potential is then varied to determine the energy spread of the electron beam. A plot of the collector current versus retarding potential is shown in fig. 6. The energy spread is

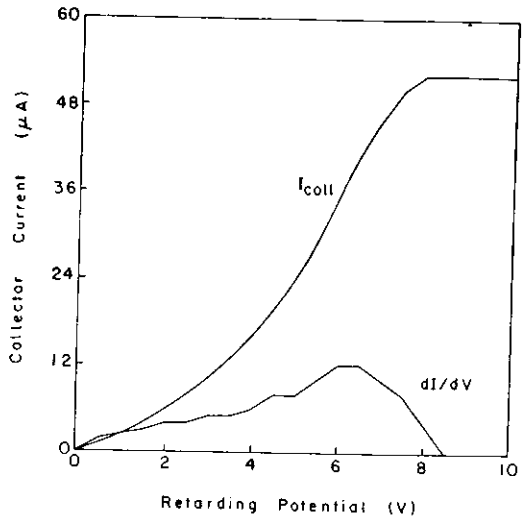

Fig. 6. Energy analysis of electron beam in the absence of laser pulses.

determined by the derivative of this plot, also illustrated in the figure.

During the experiment, the retarding potential is set to 0 V, whereby the majority of the untrapped electrons are prevented from arriving at the collector. Energy analysis of the trapped electron signal is accomplished similarly by varying the retarding potential and recording the peak current. The ratio of the peak current to

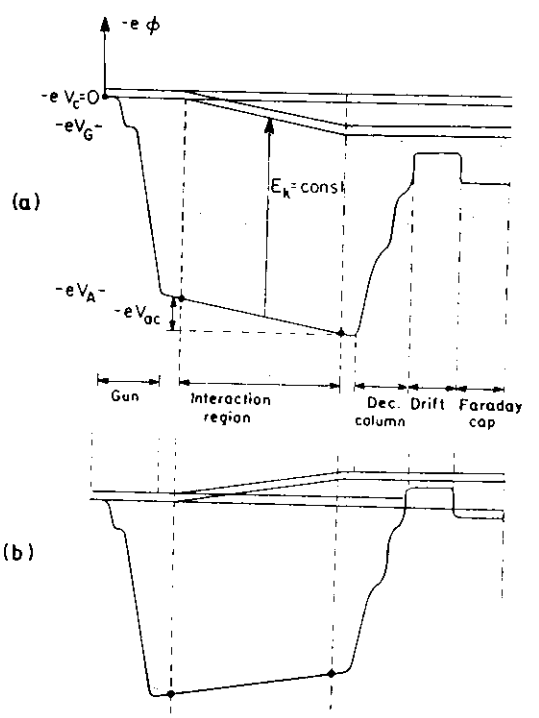

Fig. 7 Potential diagrams: (a) Acceleration; (b) Deceleration.

the total current gives the percent electrons trapped.

Potential diagrams for acceleration and deceleration along the entire electron path are illustrated in figs. 7a and 7b, respectively. Both figures show the energy separation between trapped and untrapped electrons. As seen in fig. 7b, untrapped electrons are rejected by the retarding potential.

The signal and wiggler fields are produced by two CO_2 TEA (transversely excited atmospheric) pulsed lasers. Each laser operates at a different vibrational transition to provide the difference in wavelengths. The TEA lasers emit 150 ns pulses, each directed through the interaction region and aligned with the aid of small alignment rings. In general, TEA lasers operate near atmospheric pressure, and many longitudinal modes exist. Single longitudinal mode (SLM) operation (single frequency) of the wiggler field was obtained by injection of a continuous CO_2 laser operated at SLM, as shown in fig. 4.

The signal laser is tuned with a grating to operate in the (00°1) – (0.2°0) band, at a wavelength between 9.1 and 9.4 μm. Single longitudinal model operation of the signal laser is accomplished by incorporation of a Fox–Smith interferometer [12] in the laser cavity (left side of the signal laser in fig. 4), which acts as a filter for unwanted longitudinal modes. In addition, both lasers must operate in a single transverse mode (Gaussian beam profile) to enable optimal overlap with the electron beam throughout the interaction region. The Rayleigh lengths of the laser beams were adjusted to optimize the effect of the ponderomotive potential in the interaction region.

5. Data acquisition

The electron current collected by the Faraday cup is amplified in two stages, the second of which incorporates a high pass filter. The output of the amplifier is connected to either a Tektronix 7633 storage oscilloscope, a high speed Tektronix 7912AD programmable digitizer, or a HP 54200A/D digitizing oscilloscope.

The optical pulses do not always arrive synchronously, due to the timing Jitter (50–300 ns) of the TEA lasers. It is thus necessary to perform single-shot recording of both lasers and the electron current for processing of the data. As mentioned previously, the lasers can operate in a single longitudinal mode or in several

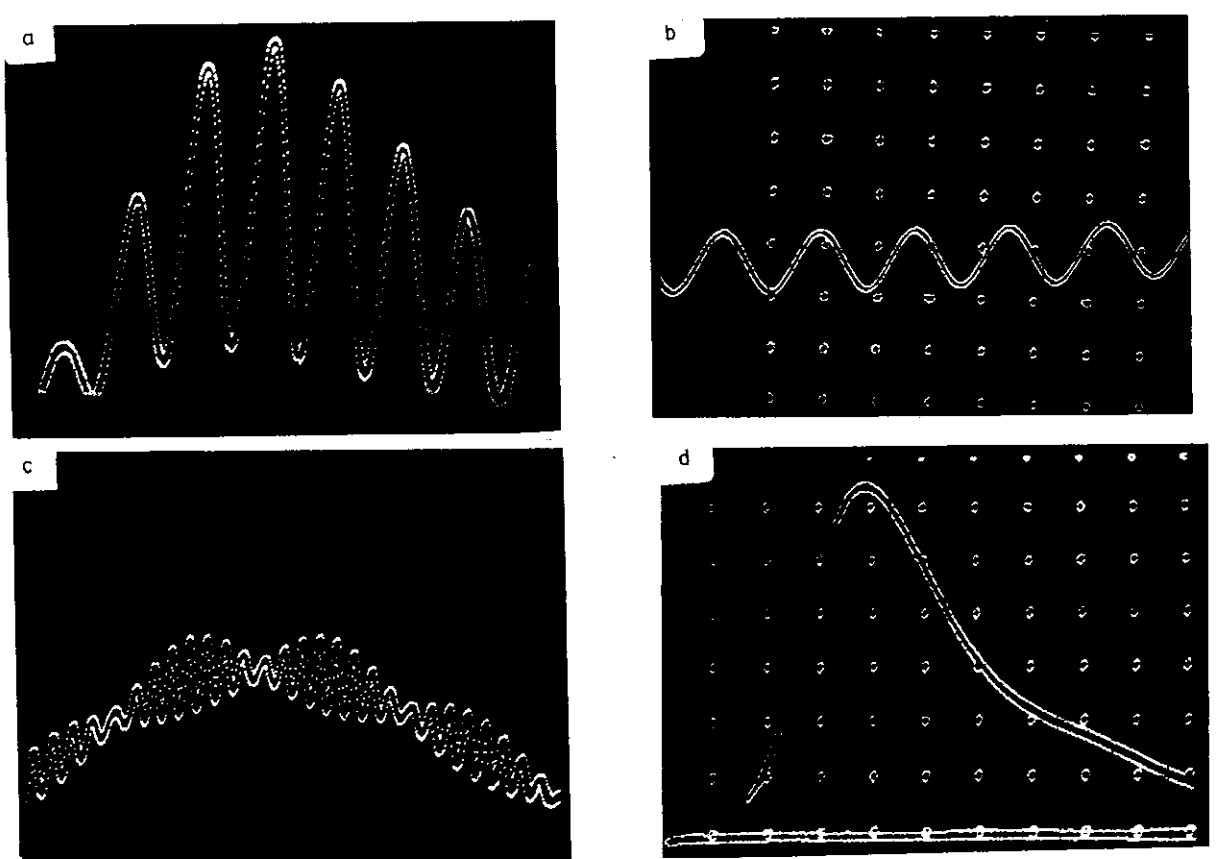

Fig. 8. Lower pulse shapes for different mode contents: (a) Two modes in laser cavity (10, 20 ns/div); (b) Two modes in Fox–Smith cavity (1 ns/div); (c) Modes in both cavities (10 ns/div).

simultaneous modes. Determination of the modal characteristics of the lasers requires a high speed, large bandwidth, single-shot recorder. We utilized the Tektronics 7912AD programmable digitizer for both high-speed viewing, and recording of experimental data. Different longitudinal modes of the TEA lasers, shown in figs. 8a–8d, well ilustrate the high speed, large bandwidth requirements. The different modes are achieved by varying the potential applied to a piezoelectric crystal (PZT), which in turn varies the cavity length of the Fox–Smith interferometer. The beats of two adjacent longitudinal modes (wavelengths) of the 2 m signal laser cavity ($\nu = c/2L = 75$ MHz) are shown in fig. 8a. Fig. 8b illustrates the beats of two adjacent modes of the 15 cm Fox–Smith cavity ($\nu = c/2L = 1$ GHz). By judicious adjustment of the PZT, it was possible to obtain three modes which result in the beats of both cavities, as shown in fig. 8c. Appropriate adjustment of the PZT forces oscillation of a single longitudinal mode, as shown in fig. 8d.

Recording and on-line processing of the data is accomplished with the aid of a PDP-11 microcomputer. The digitizers are linked to the PDP computer by means of a GPIB bus.

Table I
Free electron trapping experiment parameters

Baseline parameters		
Input signal power P_s	2.5×10^5	(W)
Input wiggler power P_w	2.5×10^5	(W)
Coil resistance	0.13	(Ω/m)
Coil current	500	(A)
Signal wavelength λ_s	9.261×10^{-6}	(m)
Wiggler wavelength λ_w	1.059×10^{-5}	(m)
Energy spread (fwhm) $\Delta\gamma mc^2$	6	(eV)
Signal waist w_{0s}	10^{-3}	(m)
Wiggler waist w_{0w}	10^{-3}	(m)
Interaction length	0.6	(m)
Interaction time	150	(ns)
Calculated parameters		
Ponderomotive wavenumber k	1.272×10^6	(l/m)
Wiggler Rayleigh length	0.2967	(m)
Signal Rayleigh length	0.3394	(m)
β	0.06702	
e velocity	2.013×10^7	(m/s)
Accelerating field E_{a0}	65	(V/m)
Initial potential	1.153×10^3	(V)
Ponderomotive field E_p	369.7	(V/m)
HW trap (no field) $\delta\gamma_t^0$	1.639	(V/m)
HW trap $\delta\gamma_t$	1.409	(eV)
Resonant phase ψ_r	0.1768	(rad)
Interaction length	0.6	(m)
Electron current	3×10^{-4}	(A)
Noise current	5×10^{-7}	(A)
Potential drop V_{a0}	39	(eV)

The calculated percentage of electrons trapped is 24.1%.

6. Experimental results

The experiment parameters are given in table 1. The two laser pulses are synchronized so as to arrive simultaneously during the electron pulse, and are shown in figs. 9a and 9b. The effect, as first observed, of the electron trapping resulting from the laser pulses is shown in fig. 9c. The peak of the trapped electron pulse shown corresponds to a trapping efficiency of 2%. As seen, the minimum (noise equivalent) trapping efficiency detectable by the system is 0.1%. When we reduced the electron beam current from 500 to 50 μA, the trapping efficiency increased from 2% to nearly 25%. This may be explained by elimination of energy spread associated with space charge effects at the larger currents. The time delay (50–100 ns) between the laser pulses and the trapped electron pulse is due to the time required for the electrons to traverse the deceleration region, and to arrive at the electron collector (Faraday cup).

The pictures in figs. 10a–10c show simultaneously

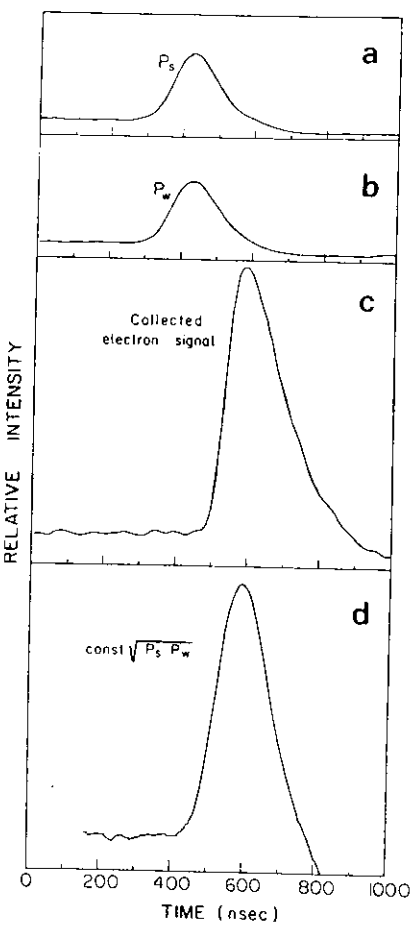

Fig. 9. Trapping effect: (a) Signal laser pulse, (b) Wiggler laser pulse; (c) Trapped electron pulse; (d) Fourth order root of wiggler and signal pulses product (displaced).

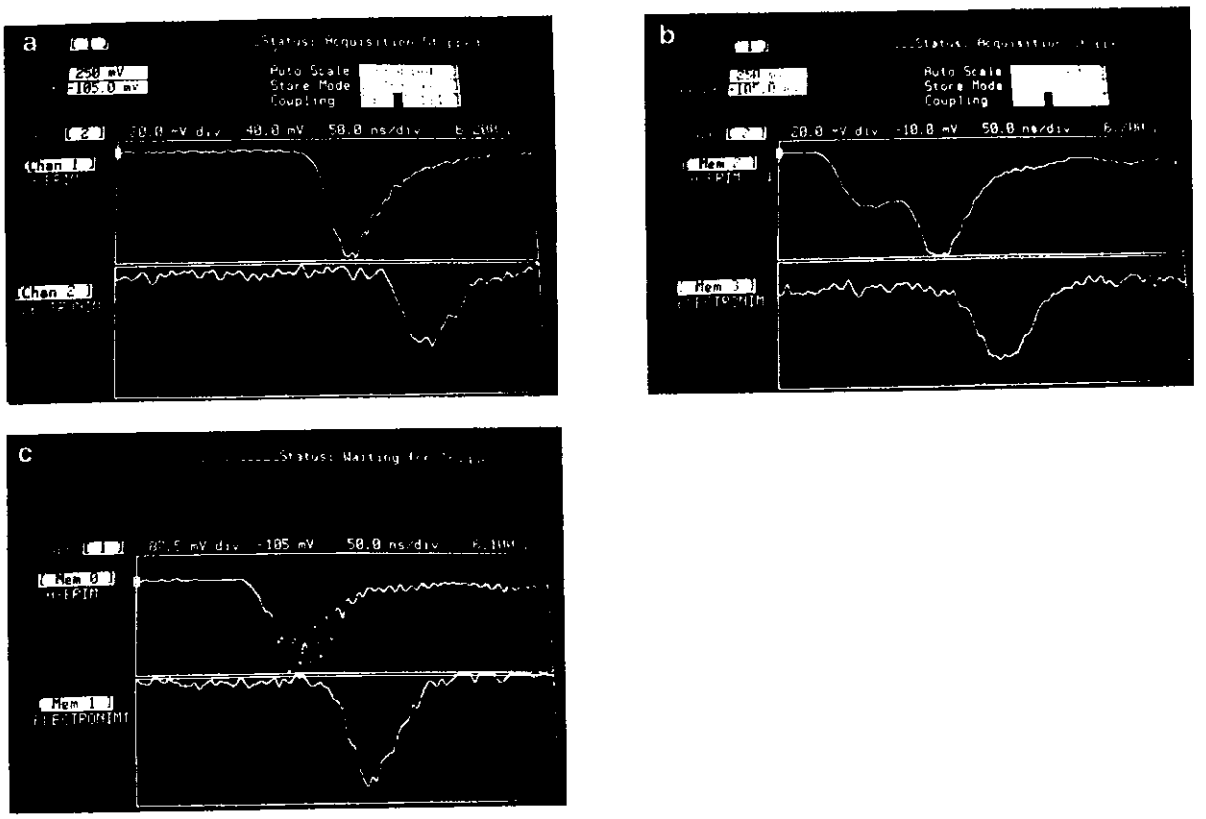

Fig. 10. Simultaneous recording of the laser pulses and trapping effect (Upper Traces: sum of two laser pulses; Lower traces: trapped electron current pulse): (a) Simultaneous laser pulses; (b) Partial temporal laser overlap; (c) Multiple longitudinal mode operation of lasers.

the sum of the two laser pulses (upper trace) and the trapped electron current pulse (lower trace). As illustrated, trapping also occurs both when there is only a partial temporal overlap of the lasers (fig. 10b) and when the lasers operate in multiple longitudinal modes (fig. 10c).

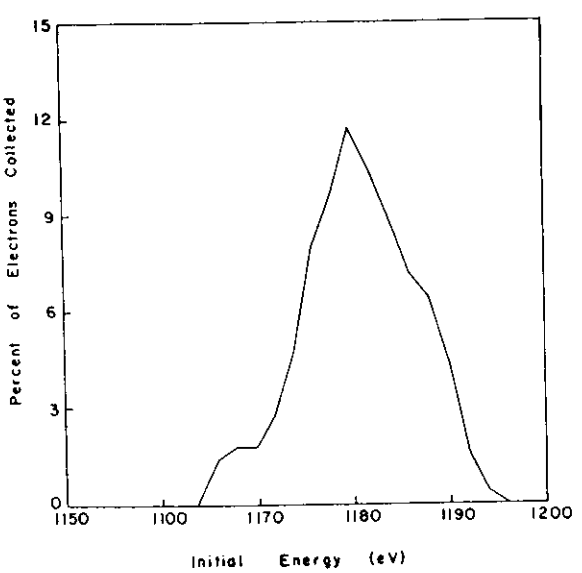

Fig. 11. Trapping efficiency vs initial electron energy.

A scan was performed of the trapping efficiency versus the position along the interaction region where the electron velocity and the ponderomotive potential wave were in resonance. This was accomplished by varying the initial electron energy. Results for a scan with a 300 A coil current are shown in fig. 11. The range of potentials that showed trapping seem to indicate that trapping occurred throughout the entire interaction region.

7. Discussion

The trap depth for weak axial field is proportional to the fourth root of the product of the laser pulse intensities (eq. (9b)). As seen in fig. 9d, there is a high degree of correlation between the calculated trapping potential and the trapped electron signal.

As previously mentioned, the width of the energy spectrum of the electrons receiving energy from the radiation field (fig. 11) corresponds to trapping throughout the interaction region. This result was unexpected since electrons must be synchronous with the

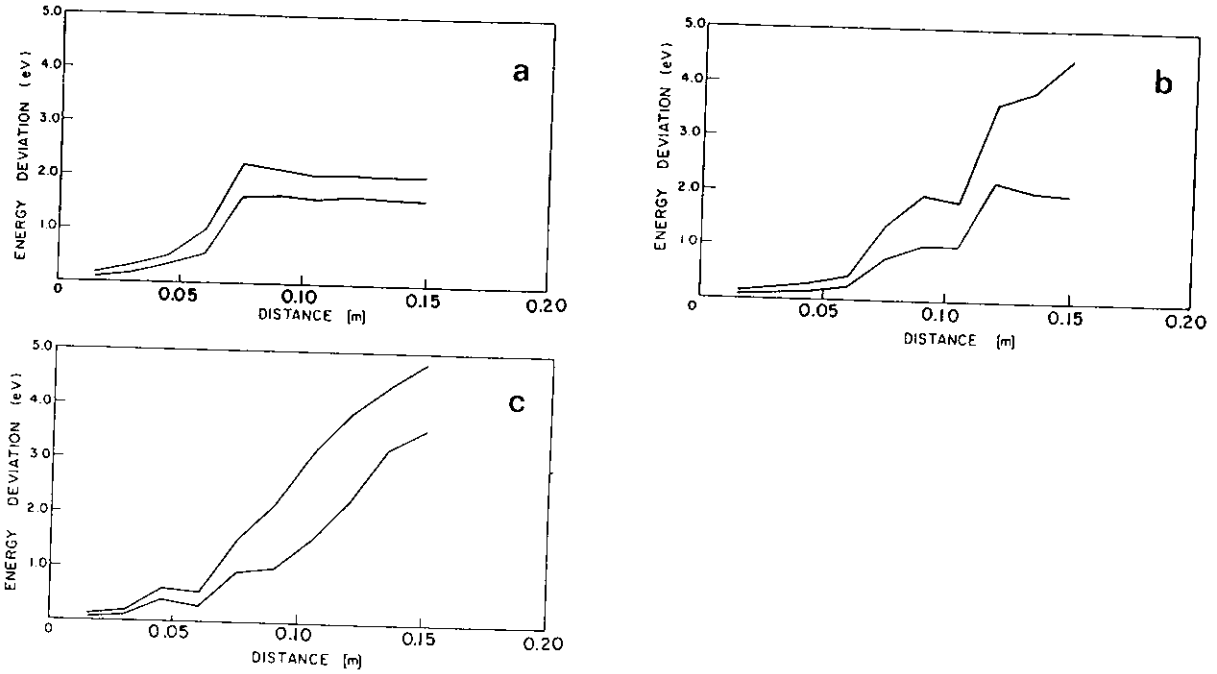

Fig. 12. Trapping simulation: (a) Single longitudinal mode operation of lasers; (b) and (c) Multiple longitudinal modes operation.

ponderomotive wave at the entrance to the interaction region in order to obtain full trapping by perfectly coherent waves; hence the resonant trapping curve of fig. 11 would be expected to have only the width of the initial energy spread of the beam ($2\Delta E = 6$ eV).

Two possible processes could explain acquisition of energy by the electrons from the radiation field along the entire interaction length. One possible process is trapping by the ponderomotive potentials of multimode radiation fields, for which the buildup time of the ponderomotive potential is quite short (corresponding to a multimode beating time) and may occur throughout the interaction region. Another possible process is the "phase displacement" electron acceleration process [19]. In this process, electrons near resonance with the potential traps are "quasi-trapped": They are forced to follow long open trajectories with energies close to the trapping energy without ever entering the closed trajectories inside the separatrix. During the dwelling time around the traps, some electrons will experience a reduced net deceleration by the axial field. A description and some results of a multimode trapping simulation of our experiment was previously reported [10]. Results of this simulation for the experimental parameters table 1 are given in figs. 12a–12c. The simulation computes the electron energies for various initial phases along the interaction region. The laser induced deviation of the electron energies relative to a freely decelerating electron is plotted in fig. 12a for the single mode case, and figs. 12b and 12c for the multimode case. In each case resonance with the ponderomotive wave occurs at 7 cm. The two curves correspond to one and three energy standard deviations with respect to an electron uneffected by the laser beams. Note that for single mode operation (where only the phase displacement process explanation would be valid) the energy deviation (spread) effect is localized at the region of resonance, whereas for the multimode case, energy transfer between the lasers and the electrons is continued after the point of resonance. Currently, we do not have a conclusive determination as to which of the electron trapping or energy transfer and spread processes plays the major role in the collected current resonance effect that we measured in our experiment. Further measurements are planned to investigate the peculiar quasi-trapping characteristics.

Acknowledgements

Initial funding for this research was supported by a USAF grant No. AFOSR 82-0239. Support was also given from the Kranzberg Institute. We would like to express our appreciation to A. Eichenbaum, B. Cohen and P. Yogev for their assistance.

References

[1] R.H. Pantell, G. Soncini and H.E. Puthoff, IEEE J. Quantum Electron. QE-4 (1968) 905.

[2] V.P. Sukhatme and P.W. Wolff, J. Appl. Phys. 44 (1973) 2331.
[3] P. Sprangle and A.T. Drobot, J. Appl. Phys. 50 (1979) 2652.
[4] P. Sprangle, C.M. Tang and W.M. Manheimer, Phys. Rev. A12 (1980) 302.
[5] N.M. Kroll, P.L. Morton and N,M. Rosenbluth, Physics of Quantum Electronics 7, eds., S. Jacobs, H. Piloff, M. Sargent III and M. Scully (Addison-Wesley, New York, 1980) p. 89.
[6] A. Gover, C.M. Tang and P. Sprangle, J. Appl. Phys. 52 (1982).
[7] H.R. Hiddleston and S.B. Segall, IEEE J. Quantum Electron. QE-17 (1981) 1495.
[8] N.M. Kroll, P.L. Morton and M.N. Rosenbluth, ibid. [5], p. 89.
[9] P. Sprangle, L.M. Tang and W.M. Manheimer, ibid. [5], p. 89.
[10] S. Ruschin, A. Friedman and A. Gover, IEEE J. Quantum Electron. QE-20 (1984) 1079.
[11] A. Gover, S. Ruschin, R. Olshan, H. Kleinman, A. Friedman and B. Steinberg, Nucl. Instr. and Meth. A287 (1985) 225.
[12] P.W. Smith, IEEE J. Quantum Electron QE-2 (1966) 666.
[13] N.M. Kroll, P. Morton and M.N. Rosenbluth, IEEE J. Quantum Electron. QE-17 (1981) 1436.

VI. EXPERIMENTS: PLANNED/IN PROGRESS